Hindawi Publishing Corporation
Advances in Tribology
Volume 2013, Article ID 850473, 11 pages
http://dx.doi.org/10.1155/2013/850473

Research Article

Atomistic Frictional Properties of the C(100)2x1-H Surface

Paul M. Jones,[1] Huan Tang,[1] Yiao-Tee Hsia,[2] Xiaoping Yan,[1] James D. Kiely,[3] Junwei Huang,[1] Christopher Platt,[1] Xiaoding Ma,[1] Michael Stirniman,[1] and Lang Dinh[1]

[1] *Seagate Technology LLC, 40710 Kato Road, Fremont, CA 94538, USA*
[2] *Western Digital Corporation, 5863 Rue Ferrari, San Jose, CA 95138, USA*
[3] *Seagate Technology LLC, Recording Heads Operations, 7801 Computer Avenue South, Bloomington, MN 55435, USA*

Correspondence should be addressed to Paul M. Jones; paul.m.jones@seagate.com

Received 3 August 2012; Accepted 5 November 2012

Academic Editor: Bruno Marchon

Density functional theory- (DFT-) based ab initio calculations were used to investigate the surface-to-surface interaction and frictional behavior of two hydrogenated C(100) dimer surfaces. A monolayer of hydrogen atoms was applied to the fully relaxed C(100)2x1 surface having rows of C=C dimers with a bond length of 1.39 Å. The obtained C(100)2x1-H surfaces (C–H bond length 1.15 Å) were placed in a large vacuum space and translated toward each other. A cohesive state at a surface separation of 4.32 Å that is stabilized by approximately 0.42 eV was observed. An increase in the charge separation in the surface dimer was calculated at this separation having a 0.04 e transfer from the hydrogen atom to the carbon atom. The Mayer bond orders were calculated for the C–C and C–H bonds and were found to be 0.962 and 0.947, respectively. σ C–H bonds did not change substantially from the fully separated state. A significant decrease in the electron density difference between the hydrogen atoms on opposite surfaces was seen and assigned to the effects of Pauli repulsion. The surfaces were translated relative to each other in the (100) plane, and the friction force was obtained as a function of slab spacing, which yielded a 0.157 coefficient of friction.

1. Introduction

Carbon-based surface films are now ubiquitous as frictional barriers that lower the wear rates of interacting bodies. They have found extensive use within the information storage industry as films for protecting both the hard disk surface and the sensitive read-write transducers from damage due friction during incremental and in some instances purposeful head-to-disk contact [1, 2]. Because of this industrial importance, a rich and extensive literature exists of both theoretical and experimental studies probing the fundamental properties of these complicated and diverse surface films [3, 4]. Within the range of these studies single crystal diamond surfaces have been extensively employed as models of the more important larger-scale industrial surfaces. Insight gained from these studies has helped the community understand surface energetic processes, including the recent manifestation of super lubricity of hydrogen-covered surfaces [5, 6].

Carbon films deposited under energetic conditions assume complicated amorphous structures, which depend on the exact conditions of deposition. Specifically, the extent of surface wear protection has been attributed to film properties that can be tailored through the manipulation of deposition parameters, precursor materials, and postdeposition processing, the combination of which can result in films ranging from "diamond-like" to softer films. In most instances a highly dense, diamond-like film is sought [3]. One of the principal metrics used to predict this attribute is the amount of tetrahedrally bound carbon-to-carbon atoms contained within the film. This important metric is found to correlate to many important mechanical and electronic properties, including film hardness, density, and optical gap [7, 8].

Recently high quality hydrogenated diamond surfaces have been proposed for use as cathode materials where their negative electron (NEA) affinity makes them a highly effective and robust material [9–11]. Previous ab initio theoretical studies have elucidated the NEA mechanism as due to the strong bonding of hydrogen to the surface π C=C bonds on the reconstructed diamond surface [12, 13]. It is believed that these surface electronic states are also observed in the super

lubricious state between two hydrogen-covered diamond surfaces [6, 14]. The mechanism for the marked decrease in interfacial friction on hydrogenated carbon surfaces has been further elucidated with surface spectroscopy and tight-binding quantum mechanical methods [15] showing that the bonded hydrogen atom passivates the carbon dangling bonds at the surface, thereby decreasing the adhesive interaction between surfaces [16]. Fluorination of these surfaces has also been explored in an effort to further reduce the coefficient of friction (COF); in particular it was noted that the significant accumulated negative charge on the surface fluorine atom and its tight surface structure, due to strong lateral interactions, lead to a strong repulsive force between interacting surfaces (larger than when hydrogen terminated) [17]. This decrease in friction between interacting surfaces can have far ranging industrial and environmental importance [5, 18, 19].

The frictional properties of diamond and other crystalline surfaces have been probed with both classical methods and ab initio-based calculations [6, 14, 20–22]. Typically, a slab model of the interacting surface is created that incorporates not only the crystalline features of the surface facet under investigation but also enough material bulk to accurately model the desired properties while remaining computationally tractable. Classical methods usually entail solving Newton's equations of motion under time-dependent conditions and allowing the use of very large material models that has been extensively and profitably applied to the hydrogenated diamond surfaces by Harrison and coworkers [20, 23]. The subject of this report is the application of density functional theory- (DFT-) based ab initio calculations to the interaction of hydrogenated C(100)2x1 surfaces by probing the electronic and bonding structure changes during the frictional interaction of these surfaces. The main thrust of this work will then be the movement of electronic charge during the surface-to-surface interaction and the nature of the commensurate repulsive state between the surfaces.

2. C(100)2x1-H Model and Computational Method

We start our discussion of the slab model used in this calculation by first considering the relaxed (100) surface of diamond, which contains unsaturated dimers with significant carbon-carbon double bond character that has been successfully functionalized with a Diels-Adler reaction [24]. The C(100) surface is one of the high surface energy facets and is one of the growth faces of DLC surface films. Its cleavage energy is highest amongst the principal diamond surface planes, and its surface chemistry and interesting electronic structure are principal reasons for using it as the focus of our study [25, 26].

As preparation for the study of surface-to-surface interactions we assembled a C(100)2x1 slab model of the diamond surface (before hydrogenation) and calculated its relaxed geometry and electronic states (model and results are not shown as this study is focused on the hydrogenated surface). This model contained eight layers of carbon atoms (not including the dimer) in a large vacuum space that was set at forty times the layer spacing to ensure minimal effects of slab-to-slab interactions. DFT ab initio theory, as implemented in the DMOL code [27, 28], was used to probe the electronic and geometric effects important in the interaction of surfaces. This implementation of density functional theory is a total electron calculation and does not use pseudopotentials or frozen electron cores. The three-dimensional cell structure was sampled using a $4 \times 2 \times 1$ grid in the Monkhorst-Pack scheme (larger sampling was explored and found not to yield any important advantage). The local density approximation (LDA) of Perdew and Wang was used for the exchange-correlation interaction to make the calculation tractable [29]. We should note that density functional theory does not treat van der Waals (vdW) interactions properly. In particular, the use of the LDA approximation for the exchange-correlation interaction (which assumes the exchange and correlation are a function of the electron density at the point of evaluation only) can lead to an overestimation of binding energies. Conversely, the generalized gradient approximation or GGA (which takes into account the gradient of the electron density at the point of evaluation) frequently underestimates the binding energy and leads to a shallow or flat adsorption profile [30, 31]. Recent efforts have been made to include dispersion forces within DFT [32, 33]. The results from these efforts generally yield an increase in the cohesive energy when compared to DFT with no correction. Since, the explicit inclusion of vdW forces increases the binding energy over the GGA result, the LDA will be used in this study because we are interested in relative changes with slab spacing and offset. A numerically derived basis was used and included polarization functions. The self-consistent field (SCF) calculations were considered converged when the largest deviation between cycles was less than 10^{-6} Hartree. To improve SCF convergence, charge smearing was allowed for orbitals within 0.01 Ha of the Fermi level. Thegeometry was considered converged based on the iterative change in bond length, energy, and force gradient (5.0×10^{-3} Å, 2×10^{-5} Ha, and 1×10^{-2} Ha/Bohr, resp.). The carbon atoms in the bottom layer of this model were held fixed for all calculations while all other carbon atoms were allowed to relax. The results of this optimization clearly show the presence of the surface dimer structure with a calculated bond length of 1.39 Å, which is approximately the length of the carbon-carbon bond in C_2H_4, and are in good agreement with previous ab initio calculations that explored this surface [13].

The electronic structure of the hydrogen-covered C(100)2x1 surface has been previously explored by various authors who found that the monolayer covered surface is the most stable [13, 30]. To begin the exploration of the hydrogen interaction with the C(100)2x1 surface, the previously optimized dimer surface was saturated with hydrogen atoms and optimized as described previously. The obtained optimized (relaxed) surface is shown in Figure 1(a), which highlights the interaction of the hydrogen atoms with the surface carbon atoms. The C–H and C–C bonds lengths of 1.15 Å and 1.61 Å are obtained after optimization; these lengths are similar to the bond lengths in ethane and previous calculations [13]. The electronic structure of this surface changes significantly from that observed on the clean surface. Whereas, the C(100) dimer surface density of states

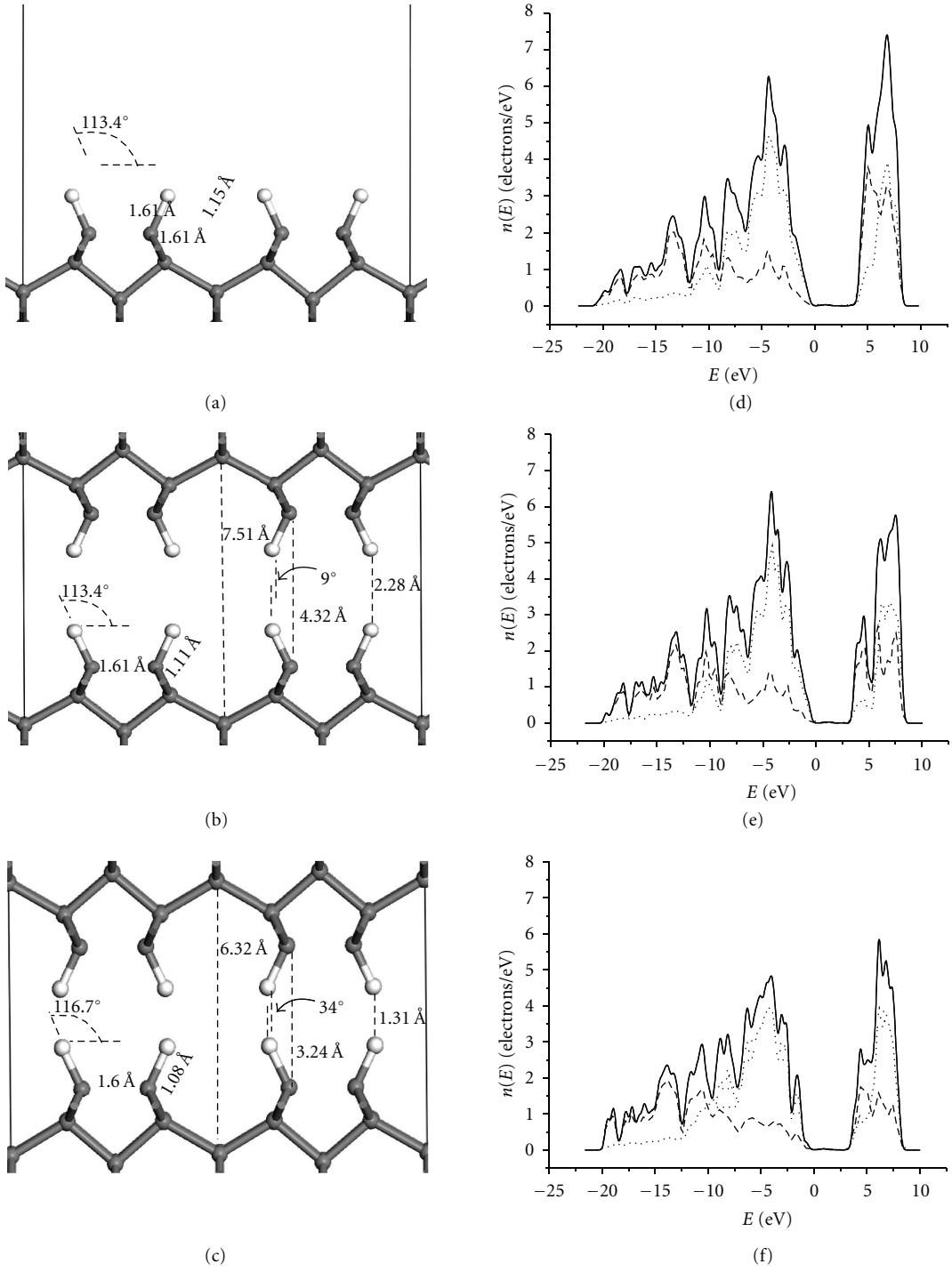

FIGURE 1: (a) Surface dimer geometry of the fully relaxed C(100)2x1-H; (b) spacing and geometry of the cohesive state between C(100)2x1-H surfaces at 4.32 Å dimer carbon-to-opposite surface dimer carbon spacing; (c) geometry of slab-to-slab repulsive state at a 3.24 Å dimer-to-dimer spacing; (d) DOS of the dimer and first carbon atom layer shown in part (a), solid line is total DOS, dashed line the s-states partial DOS and the dotted line the p-states partial DOS, VBM = 0 eV; (e) similar DOS of the cohesive state shown in part (b); (f) similar DOS of (c) the repulsive interaction between surfaces. Gray spheres represent carbon atoms and white are hydrogen atoms, in all figures.

(DOS) contains recognizable π, π^*, σ, and σ^* states, the monohydride surface DOS (see Figure 1(d), DOS obtained from the outer hydrogen and first two carbon atom layers) is well separated with a clear band gap of ~3.3 eV (DFT is known to underestimate band gaps). The σ C–H bonding states can be readily identified in the DOS peaking in the −4 eV range measured from the valence band maximum (VBM) (see Figure 1(d)) and are due to the interaction of

the hydrogen 1s and the carbon 2p states. The conduction band is largely composed of states localized on the hydrogen layer. Maps of the difference in electron density (total density minus the density due to the separate atoms) enable the visualization of the concentration or removal of electron density and are presented in Figure 2(a) as a slice through the surface carbon-hydrogen bonds parallel to the c direction. An accumulation of electron density between the dimer carbon and hydrogen atoms defines the C–C and C–H bonds. The calculated Mayer bond orders, which are 0.962 and 0.942 for the two bonds, respectively, (see Table 1), further support this visualization and indicate the reduction in the π bond character of the dimers [34]. The calculated Mulliken charge distribution places a 0.085 e positive charge on the surface hydrogen atoms and a −0.102 e charge on the carbon atoms in the dimer (see Table 1) [35]. This charge separation at the surface yields the well-known dipolar layer observed in other similar calculations and is the mechanism behind the NEA observed on this surface. The formation of the surface dipole moment is also thought to be an important contributor to the surface reactivity, conductivity, and wetting characteristics of this surface [36]. The lowest energy electronic orbital dominantly centered on the dimer is due to the σ C–C bond (see Figure 2(d)). The highest occupied orbital dominantly centered on the C–H bond (shown in Figure 2(e)) is obviously composed of hydrogen 1s and C 2p components and shows that this orbital overlaps neighboring hydrogen atoms.

Thus the hydrogen-saturated C(100)2x1 surface contains a surface dipole layer whose aliphatic nature is revealed in its electronic structure. The outlined changes in this surface electronic structure from one dominated by olefinic character, and its resultant facile chemistry, to a dominantly aliphatic surface, makes further surface chemistry difficult and contributes to the known stability of this surface.

3. Results and Discussion

3.1. Approach of the C(100)2x1-H Slabs. To begin our study of the friction between two C(100)2x1-H surfaces, we have placed two of the previously described hydrogenated surfaces facing one another in a large vacuum space to minimize unwanted interactions. We have frozen the outer carbon layers in each slab and allowed all other layers, including the surface hydrogen atoms, to relax as the slabs are brought incrementally and commensurately closer together. Figure 1(b) illustrates the arrangement of the slabs and defines the distance between them as the distance between opposing dimer carbon atoms. The surface charge distribution of the widely spaced (noninteracting) slabs does not change from the single slab result (data not shown), supporting the lack of slab-to-slab interaction at these separation distances. The DOS of the slab was checked to further assure the robustness of our scheme (the utilization of large vacuum spaces). The change in total energy as the surfaces are brought incrementally together is shown in Figure 3(a). No interaction of the surfaces is calculated until they are approximately 6.5 Å apart where a net stabilization begins and increases in strength until approximately 4 Å when the interaction becomes rapidly repulsive. The depth of the calculated stabilization at 4.32 Å is 0.42 eV (total energy of the slabs at incrementally smaller separation minus total energy of separated slabs) and is significantly larger than previous calculations of this interaction [6, 14]. However, the work of adhesion, defined as the energy to separate the two surfaces divided by the cell area (in this instance ~0.133 J/m^2), compares favorably with a previous AFM study using a hydrogen-covered diamond single crystal surface and a diamond-coated tip having approximately single atom at its apex (~0.159 J/m^2) and a more recent study on C(111) and C(001) surfaces [37, 38]. Interestingly, studies of interacting hydrogenated diamond surfaces using widely divergent ab initio theories, most using super cell methods along with pseudopotentials, have found a similar weakly bound state [6]. In contrast, calculations using small molecules as models of the surface interaction along with Hartree-Fock methods yield only a strong repulsive barrier [39]. The divergence in these calculated results shows the need for an adequate slab size to correctly model this weak interaction.

Thus, the compression of the C(100)2x1-H surfaces (see Figure 1(b)) results in a stabilized state at approximately 2.28 Å (hydrogen atom-to-opposing hydrogen atom) separation (or 4.32 Å carbon atom-to-opposing carbon atom in the dimers, see Figure 1(b)) and thereafter a strong interlayer repulsion.

The surface geometry of the cohesive configuration (see Figure 1(b)) changes little from the C(100)2x1-H surface. The C–H bond at 1.11 Å has contracted by approximately 0.04 Å from the free surface and correlates with the larger charge separation in the dimer in this configuration (vide infra) while the C–C bond length remains at its free slab value of 1.61 Å as does the H–C–C angle 113.4°. Interestingly, the angle between C–H bond pairs on opposite slab surfaces is approximately 9° and signals the incipient effects of slab-to-slab repulsion, especially on the C–H bond. Significant changes in the distribution of charge near the surface take place as the slabs have been incrementally brought into near contact. In this geometry, which is weakly cohesive, approximately 0.04 e (net +0.125 e) is transferred from the hydrogen atoms to the carbon atoms in the dimer (net −0.144 e), thereby increasing the charge separation and hence the surface dipole moment (see Table 1). The increased surface dipole has little effect on the peak due to the σ C–H states at approximately 4.5 eV below the VBM. The rest of the valence band (see Figure 1(e)) also changes little from the VB of the separated state. In contrast, the shape of the conduction band changes to a distinct two-peak structure with the lower edge of the band at approximately 3.0 eV. It is dominantly composed of empty hydrogen 1s states (see Figure 1(e)). The electron density difference maps shown in Figure 2(b) portray an increase of density between the carbon atoms in the surface dimer and an increase centered on the hydrogen atoms, which is similar to the density map of the separated slab (see Figure 2(a)). Increasing the range of the displayed density difference (see Figure 2(b) inset), however, reveals a somewhat larger increase in density centered between the dimer carbons for the stabilized configuration and a slightly

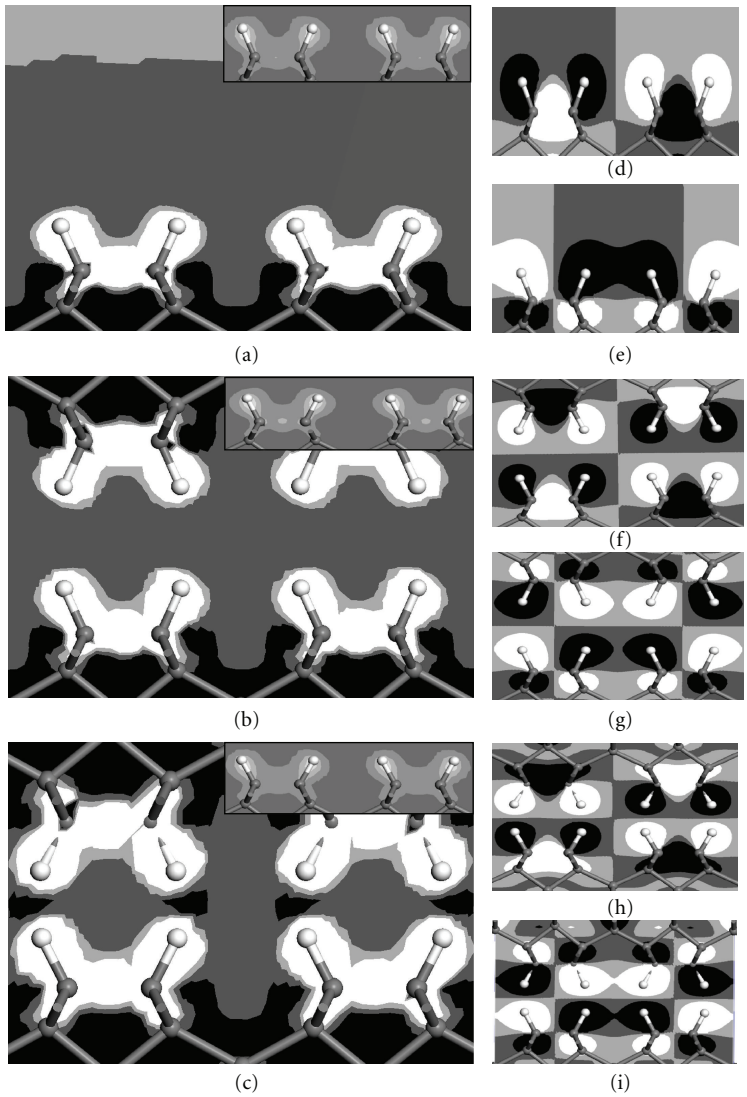

Figure 2: (a) Electron density difference map through the C–H bonds in the dimer parallel to the *c*-axis of the C(100)2x1 slab, black = (−10%) to (−5%), dark gray = (−5%) to (0%) density loss, light gray = (0%) to (5%), and white = (5%) to (10%) density gain, inset is the same map with −100% to +100% in four equal steps from density loss to gain as in part (a) and shows little density build up; however, some +25% ±25% density difference light gray areas are slightly visible between the carbon atoms in the dimer. (b) Electron density map through the C–H bonds on the upper and lower slabs dimers when at a separation with a net cohesive stabilization, electron density difference color scheme is the same as part (a); inset is map through the lower slab dimer C–H with color scheme as in inset to part (a), showing more electron density build up between the C–C atoms in the dimer than (a). (c) Electron density map through the C–H bonds on the upper and lower slab dimers at a separation having a net repulsive interaction, electron density difference color scheme is the same as part (a) black patches between opposing dimer hydrogen atoms, has negative electron density difference, and is assigned to Pauli repulsion at this separation; inset is map through the lower slab dimer C–H with color scheme as in inset to part (a), showing no electron density build up between the C–C atoms in the dimer. (d) Map of the highest occupied orbital centered on the dimer on the C(100)2x1-H surface through the C–H bonds and parallel to the *c*-axis, darker colors are negative phase and lighter colors the positive; steps plotted are from −0.02 to −0.01, −0.01 to 0, 0 to 0.01, and 0.01 to 0.02 electron/Å^3; orbital is dominantly due to the σ C–C bond with highest values between the carbon atoms. (e) Map of the highest occupied orbital centered on the C–H on the C(100)2x1-H surface through the C–H bonds, color scheme is the same as in part (d); orbital is dominantly due to the σ C–H bond with some overlap between neighboring hydrogen atoms on different dimers. (f) Similar map of the highest occupied orbital centered on the dimers on the C(100)2x1-H surface-to-surface interaction at a separation having a net cohesive stabilization, orbital is dominantly due to the σ C–C bond that has changed little from part (d). (g) Similar map of the highest occupied orbital centered on the C–H when slabs have net cohesive stabilization; orbital is dominantly due to the σ C–H bond with no overlap between neighboring hydrogen atoms on different dimers. (h) Similar map of the highest occupied orbital centered on the dimer when the slabs are experiencing a repulsive interaction; orbital is dominantly due to the σ C–C bond now having high orbital values moved from between the carbon atoms to beneath and outside of the C–C bond. (i) Similar map of the highest occupied orbital centered on the C–H when the interacting slabs experience a net repulsion; orbital is dominantly due to the σ C–H bond now with some overlap between neighboring hydrogen atoms on different dimers.

Table 1: The geometry, charges, and the Mayer bond order of the dimer, for the C(100)2x1-H surface, the C(100)2x1-H//C(100)2x1-H slabs interacting at a separation that is cohesive (net stabilized), and these slabs at a smaller repulsive separation.

Dimer	C(100)2x1-H slab				C(100)2x1-H//C(100)2x1-H (cohesive)				C(100)2x1-H//C(100)2x1-H (repulsive)			
	Bond length (Å)	Angle	Bond order	Charge (e)	Bond length (Å)	Angle	Bond order	Charge (e)	Bond length (Å)	Angle	Bond order	Charge (e)
C–C	1.61	na	0.963	na	1.61	na	0.962	na	1.60	na	0.933	na
C–H	1.15	na	0.942	na	1.11	na	0.947	na	1.08	na	0.933	na
H–C–C	na	113.4°	na	na	na	113.4°	na	na	na	116.7°	na	na
$H–C_{up}/H–C_{down}$	na	na	na	na	na	9°	na	na	na	34°	na	na
C	na	na	na	−0.102	−0.144	na	na	−0.144	na	na	na	−0.147
H	na	na	na	+0.085	+0.125	na	na	+0.125	na	na	na	+0.129

more density centered on the hydrogen atoms for this configuration (compare inset in Figures 2(a) and 2(b)). The orbitals centered on the dimer allow a fuller description of a potential interaction between the slabs. Figures 2(f) and 2(g) present the highest occupied level centered on the σ C–C and the C–H bonds, respectively. Little change can be seen in the σ C–C when compared to the same orbital on the separated slab in Figure 2(d). The spatial extent of the σ C–H orbital, shown in Figure 2(g), appears to be at least qualitatively contracted so that it no longer overlaps at neighboring hydrogen atoms on different dimers. This may be due to the previously noted increase in net positive charge on the hydrogen atom in this geometry. The Mayer bond order of the dimer C–C bond is 0.962, which is the same as for the separated slab. The C–H bond order is 0.947, a slight increase from the separate slab.

Thus, as the slabs incrementally approach one another, a shallow energy minimum is observed at 4.32 Å, which has a surface geometry similar to that calculated on the separated slab but with a slightly contracted C–H bond and an approximately 9° angle between C–H bonds on opposite surfaces. An additional transfer of charge from the hydrogen atoms to the carbon atoms takes place in the dimer. An increase in electron density between the carbon atoms in the dimer is observed along with a more subtle increase at the hydrogen atoms (compared to C(100)2x1-H). The highest occupied electronic state centered on the C–H reveals a decrease in the interdimer overlap at neighboring hydrogen atoms on the same surface, which we assign to the increased positive charge at the hydrogen atom center contracting the spatial extent of the orbital at that site.

Further compression of the layers rapidly decreases the difference in total energy and becomes highly repulsive (see Figure 3(a)). Figure 1(c) presents the geometry of a configuration along this repulsive end of the curve at an interslab distance of 3.24 Å (between opposite dimer carbons) as an illustrative example. The dimer C–C bond length at 1.60 Å has changed little; in contrast the C–H bond has further contracted to approximately 1.08 Å. Perhaps more important than these bond length changes are the changes in the overall dimer geometry on the surface. Of these, the most dramatic is the large increase in the angle between the opposing C–H bonds (see Figure 1(c) and Table 1) to approximately 34° and shows the effect on the C–H bond due to the compression of the surfaces. This dramatic effect has been previously discussed based on molecular dynamics (MD) calculations, where it was noted that at higher compression the opposing hydrogen atoms in the C–H bonds "revolve" around each other to minimize their contact [40]. A significant bending of the C–H bond in the dimer toward the slab surface (H–C–C angle increases to 116.7°, see Figure 1(c) and Table 1) takes place at this slab-to-slab separation. The Mulliken charges have changed little (see Table 1). In contrast, the Mayer bond orders for the dimer C–C and C–H bonds have significantly decreased to 0.945 and 0.933, respectively, and indicate the weakening of these surface bonds due to the repulsion under the compression of the surfaces. A change in the electron density difference is also observed at this geometry. The inset in Figure 2(c) presents the difference map for this slab-to-slab spacing; it reveals no increase in density along the C–C bond thus supporting its lower bond order. Figure 2(c) shows the density difference, in a more sensitive range, where a large decrease in the electron density (black region) in the vacuum space approximately between the hydrogen atoms on opposite slab surfaces is observed. We assign this large decrease, which is not observed in either of the other geometries (compare Figures 2(a) and 2(b)), to the effects of repulsion from the Pauli principle and must be centered on or near the hydrogen atoms of the dimer. The highest occupied surface state centered on the C–C dimer is shown in Figure 2(h) where the effects of the bending of the C–H bond are especially evident. The displacement of high orbital values from the center of the C–C bond of the dimer to between the dimer carbon and the first carbon layer (compare Figures 2(d) and 2(f)), decreases the electron density between these carbon atoms. This decrease in electronic density between the carbon atom centers weakens the dimer bond and thereby decreases its bond order. We note that due to the noted "bending" of the C–H bond toward the surface the overlap of similarly phased orbitals at neighboring hydrogen atoms in the highest occupied state centered on the C–H bond in this slab-to-slab geometry is increased when compared to the stabilized configuration (see Figure 2(i)).

Thus, for slab-to-slab spacing smaller than ~4.3 Å a strong repulsion between the slabs is expected. The effect of the small spacing is to deform the geometry of the dimer by increasing the angle between pairs of upper and lower H–C bonds, indicating that the hydrogen atom pairs on opposite surfaces "revolve" around one another, while the C–H bond angle is bent toward the slab surface. These geometric changes are due to the effects of Pauli repulsion, which is clearly observed as a depleted electron density zone in the vacuum space between opposing hydrogen atom pairs, weakening the bonding within the dimer by removing electron density from the σ C–C and decreasing the C–C and C–H bonds strength.

3.2. Slab-to-Slab Atomistic Friction. To investigate the changes of friction with sliding we have adopted the theory and procedure of Zhong and Tomãnek and have translated the slabs relative to each other in the (100) plane at different interslab spacing, while relaxing the entire structure (subject to the constraints previously discussed) at each step [41]. We assume the entire two-slab structure is at equilibrium at each step in its translation across the surface by noting that the range of relative motion is small. Figure 3(b) assembles the resulting family of interaction curves obtained by this procedure. Each curve in this figure was obtained at a fixed spacing and interfacial load. As a prelude to the analysis of these curves we explored many of them over a longer sliding distance to convince ourselves that they are indeed periodic (with period ~2.5 Å) and have no more structure than is shown in Figure 3(b). Thus all curves were obtained over approximately the same relative range, which encompassed the maximum and minimum of the interaction curve and therefore represents the full range of the surface potential corrugation. In general, the curves pass through a maximum as the hydrogen atoms on opposing surfaces are aligned. The depth (energy maximum to minimum) of the curves increases with load and is reflective of the increasing

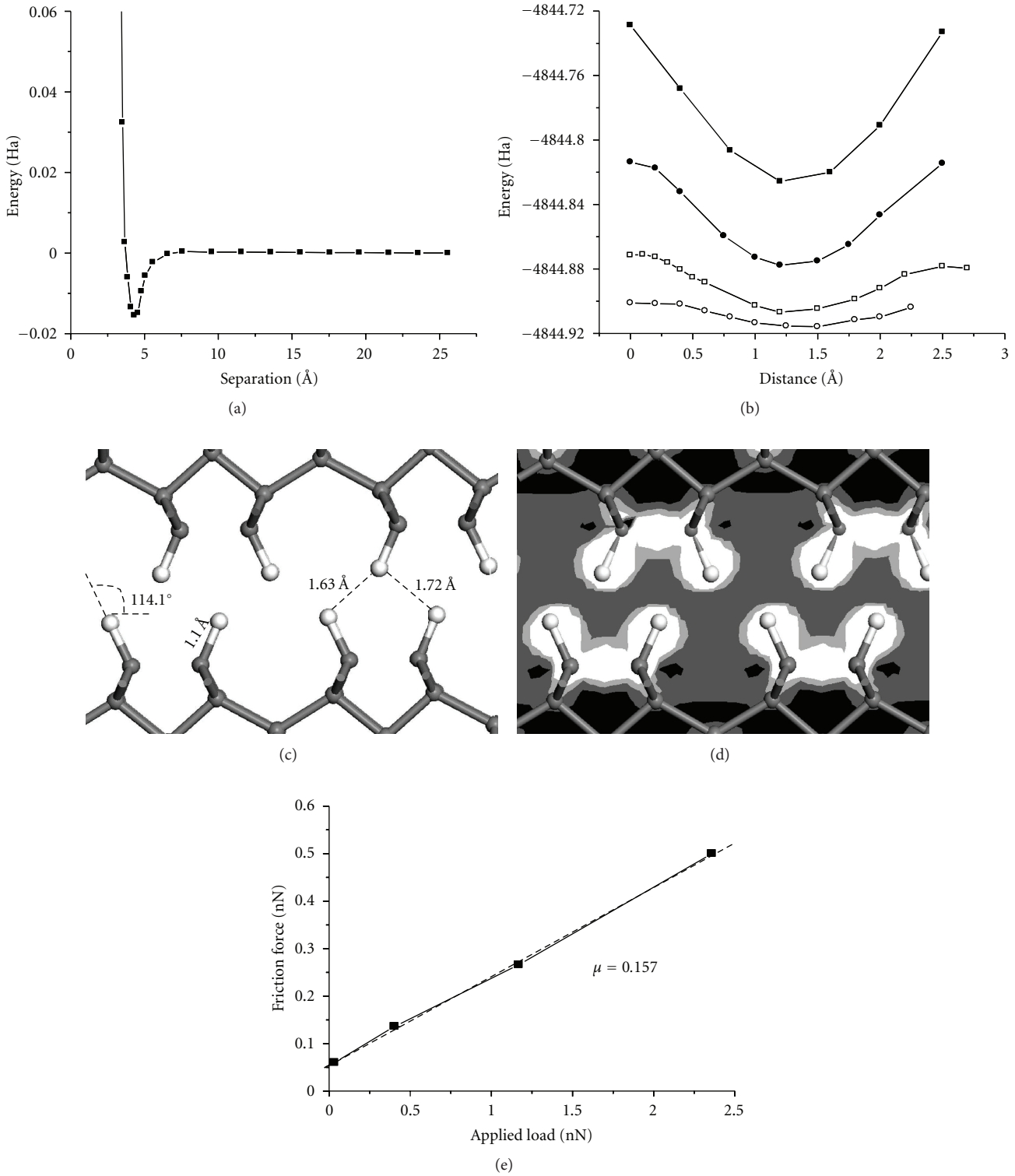

Figure 3: (a) The total energy difference (with separated configuration at 25 Å) of two C(100)2x1-H surfaces with incrementally decreasing separation, a cohesive interaction at approximately 4.5 Å separation is observed with increasingly repulsive interactions at smaller spacing (distance as measured between the carbon atoms of the dimer between upper and lower surfaces). (b) Total energy of interaction of C(100)2x1-H surfaces at fixed distance and load while surfaces are slid in the (100) plane: open circle load is 0.0326 nN, open square load is 0.4034 nN, solid circle load is 1.1694 nN, and solid square load is 2.3590 nN. (c) Geometry of interacting surfaces at 3.24 Å (Figure 1(c)) spacing when translated ~1.2 nm into relative minima, showing relative positions of opposing hydrogen atoms. (d) Electron density difference map of part (c) coloration as described in Figure 2(c). (e) Friction force derived from part (b) as a function of applied load, coefficient of friction is $\mu = 0.157$.

Pauli repulsion as the slabs are brought closer together. Similarly, the decreasing value of the total energy, observed as an incremental offset in the energy as more load is applied, reflects this same repulsion mechanism. We will use the previously discussed high-energy state at 2.36 nN loading (Figure 3(b)) to illustrate the effect of sliding on the geometry of the layers in the slab. Note that a significant relative stabilization is encountered as the slabs are slid from this position, at a fixed spacing, by approximately 1.2 Å. Figure 3(c) gives the geometry of this configuration. In contrast to the fully aligned and highly destabilized geometry, the geometry of this state brings the surface hydrogen atoms on each slab into positions approximately half way between those on the opposite face. In this geometry the C–H bond lengthens to 1.10 Å, and the H–C–C angle decreases to 114.1°. The net increase in stabilization is therefore highly correlated to the significant changes in this angle and must reflect the change in repulsion between the surfaces. It is well known that the net overlap of the hydrogen 1s orbital and the carbon sp3 hybrid orbital rapidly decreases as this angle increases, thus significant changes in the angle directly contribute to the calculated changes in total energy [42]. The electron density deformation maps of this geometry, shown in Figure 3(d), support this view. In contrast to the repulsive electron density difference observed between hydrogen atoms in the aligned geometry, the offset of the C–H bonds and the hydrogen atoms on opposite faces decreases this effect and allows the small relaxation of the H–C–C angle toward the equilibrium geometry on the free C(100)2x1-H surface (113.4°). In general, as the slabs are translated at fixed spacing, the noted and discussed interactions abate and then build with an approximate 2.5 Å period due to the hydrogen-to-hydrogen spacing on the surface.

The frictional force acting on the sliding surface is obtained from Figure 3(b) using Zhong's method [41]. Plotting this force versus the normal load we obtain a coefficient of friction of approximately 0.157 (see Figure 3(e)). This value is in surprising agreement with an MD calculation using a bond order potential method [43] and with AFM measurements on similar surfaces [2, 39], but is smaller than that obtained using large-scale MD simulations of Scanning Force Microscope (SFM) experiments that included an MD model of a spherical tip [44]. This range of agreement is understandable as friction at the level modeled here is velocity dependent; in contrast the present study is assumed at equilibrium at each incremental step of the opposing surfaces. Nonetheless, we note that the present results show that the friction force is linear over the load range studied, in contrast to force-field based results that are nonlinear albeit over a wider load range [20]. A residual friction force is obtained if the friction force versus load curve is extrapolated to zero in Figure 3(e) [20, 39]. However, we cannot discount a nonlinear behavior in the friction force below the range of loads probed in this report.

Regarding the size of the present coefficient of friction and its relationship to previous results, it is clear that they are on the lower end. Perry and Harrison found $\mu \sim 0.2$; though they probed a larger load range [40], and the results of an effort using DFT with pseudopotentials, plane waves, and GGA did not reveal the presence of an energy minimum at any slab-to-slab spacing. Additionally, their calculated value of $\mu \sim 0.05$ was noted as "too low" [6]. Another study that used small discrete models for the hydrogenated surface along with a Hartree-Fock method and the split valence basis sets found no energy minimum as the two-slab models approached, and the authors obtained a friction coefficient of $\mu \sim 0.22$ with apparently no residual friction force at zero load [39].

Regarding the residual friction force at zero load, popular models of adhesive microscopic friction, the JKR and DMT for example, that are routinely applied to AFM-based friction measurements each exhibit a nonzero contact area at zero load and a minimum normal load which exhibits nonzero contact [45]. Each of these nanoscale contact formulations include attractive forces (JKR short-range adhesion and DMT longer-range surface force) that are missing in the hard-wall repulsion used to derive Hertz's model. It is believed that similar adhesive forces are the source of the nonzero friction at zero load.

4. Conclusions

DFT calculations using the LDA formalism reveal a cohesive state between two C(100)2x1 surfaces passivated with a monolayer of hydrogen (at a spacing of 4.32 Å). This state is characterized by strong charge transfer from the surface hydrogen atoms to the first layer of carbon atoms in the slab and a relative strengthening of the surface C–C of the dimer. No change in the H–C–C bond angle is observed due to the lack of repulsion at this slab-to-slab spacing. No significant change in the highest occupied orbital centered on the C–H bond is observed. In fact, this state appears as the superposition of the same states on the single C(100)2x1-H surface and indicates that no direct surface-to-surface chemical bonding interaction takes place. In contrast, the repulsive interaction of the two slabs at spacing smaller than the cohesive state is characterized by significant changes in the dimer geometry that can be assigned to the influence of repulsion at this close proximity. Visualization of the effect of repulsion on the electron density is facilitated using electron density difference maps that specifically show a large decrease in density between the hydrogen atoms on opposite surfaces. Slabs set at increasingly close proximity were translated in the (100) plane with the total energy going through maxima and minima when surface hydrogen atoms are directed toward each other and between the opposing C–H bonds, respectively. No bond breaking was observed as a consequence of these movements. The coefficient of friction ($\mu \sim 0.157$) was obtained from the relationship of the calculated friction force to applied load and was found to be linear with a residual force at zero load. This residual force is assigned to the discussed cohesive state between C(100)2x1-H slabs and is consistent with pertinent theories (JKR and DMT) of nanoscale contact and friction.

Magnetic recording technology uses a rapidly evolving set of materials to obtain greater information density on the surface of the storage disk. Amongst the most important of these materials is the carbon overcoat on the storage

medium. This nanothick film protects the recorded information from environmental and mechanical degradation. Significant effort is now focused on the further densification of this surface film especially in light of the near term adoption of heat-assisted magnetic recording needed to further extend this recording technology [46]. The current study has been made as a tractable approximation to these advanced films. The C(100) surface is one of the principal growth surfaces of these COC films allowing the transferability of the principal learning from this study. The deposition of the COC takes place within a vacuum space that is likely to have a significant partial pressure of hydrogen, therefore, as these films grow under energetic conditions hydrogen is likely to saturate the surface of the finished film. Further, the C(100) is expected to be enriched at the surface and thus becomes hydrogenated. Due to the inverted dipole moment at the surface (positive end out) caused by the passivation of the dangling bonds by hydrogen and their concomitant rearrangement on the surface, a large decrease in the wetting of the surface by the widely used disk surface perfluorolubricant is anticipated [47]. This change will make it more difficult to stabilize the lubricant on the surface and keep it at the thickness required. Friction at the interface between the media COC and the read-write transducer is due to an adhesion component (modeled here) and the applied load (and obviously contains a shear component not considered in this study) [2]. There has been a large reduction in the surface roughness of each of these interacting bodies as this recording technology has progressed (now approaching near atomic smoothness ~1–3 Å average roughness). Thus, a model of asperity contact may no longer be a fully accurate model of this frictional interaction. The interaction of these surfaces at the loads used in this study do not cause damage to the surface and reinforces the fundamental role that hydrogenation plays in this result: keeping the surfaces apart at high applied loads and passivating the π dimer bonds on the reconstructed diamond surface with a reasonably inert layer.

References

[1] A. Anders, W. Fong, A. V. Kulkarni, F. W. Ryan, and C. S. Bhatia, "Ultrathin diamond-like carbon films deposited by filtered carbon vacuum arcs," *IEEE Transactions on Plasma Science*, vol. 29, no. 5 I, pp. 768–775, 2001.

[2] C. M. Mate, "Nanotribology studies of carbon surfaces by force microscopy," *Wear*, vol. 168, no. 1-2, pp. 17–20, 1993.

[3] J. Robertson, "Diamond-like amorphous carbon," *Materials Science and Engineering (R)*, vol. 37, no. 4–6, pp. 129–281, 2002.

[4] D. R. McKenzie, "Tetrahedral bonding in amorphous carbon," *Reports on Progress in Physics*, vol. 59, no. 12, pp. 1611–1664, 1996.

[5] A. Erdemir, "Superlubricity and wearless sliding in diamondlike carbon films," in *Surface Engineering 2001—Fundamentals and Applications*, vol. 697 of *MRS Proceedings*, pp. 391–403, November 2001.

[6] S. Dag and S. Ciraci, "Atomic scale study of superlow friction between hydrogenated diamond surfaces," *Physical Review B*, vol. 70, no. 24, Article ID 241401(R), 4 pages, 2004.

[7] F. Demichelis, C. F. Pirri, A. Tagliaferro et al., "Mechanical and thermophysical properties of diamond-like carbon (DLC) films with different sp^3/sp^2 ratios," *Diamond and Related Materials*, vol. 2, no. 5–7, pp. 890–892, 1993.

[8] J. T. Titantah, D. Lamoen, E. Neyts, and A. Bogaerts, "The effect of hydrogen on the electronic and bonding properties of amorphous carbon," *Journal of Physics Condensed Matter*, vol. 18, no. 48, pp. 10803–10815, 2006.

[9] L. Diederich, P. Aebi, O. M. Küttel, and L. Schlapbach, "NEA peak of the differently terminated and oriented diamond surfaces," *Surface Science*, vol. 424, no. 2, pp. L314–L320, 1999.

[10] J. van der Weide, Z. Zhang, P. K. Baumann, M. G. Wensell, J. Bernholc, and R. J. Nemanich, "Negative-electron-affinity effects on the diamond (100) surface," *Physical Review B*, vol. 50, no. 8, pp. 5803–5806, 1994.

[11] H. Kawarada, "Hydrogen-terminated diamond surfaces and interfaces," *Surface Science Reports*, vol. 26, no. 7, pp. 205–259, 1996.

[12] S. J. Sque, R. Jones, and P. R. Briddon, "Structure, electronics, and interaction of hydrogen and oxygen on diamond surfaces," *Physical Review B*, vol. 73, no. 8, Article ID 085313, 15 pages, 2006.

[13] J. Furthmüller, J. Hafner, and G. Kresse, "Dimer reconstruction and electronic surface states on clean and hydrogenated diamond (100) surfaces," *Physical Review B*, vol. 53, no. 11, pp. 7334–7351, 1996.

[14] G. Zilibotti, M. Ferrario, C. M. Bertoni, and M. C. Righi, "Ab initio calculation of adhesion and potential corrugation of diamond (001) interfaces," *Computer Physics Communications*, vol. 182, no. 9, pp. 1796–1799, 2011.

[15] K. Hayashi, K. Tezuka, N. Ozawa, T. Shimazaki, K. Adachi, and M. Kubo, "Tribochemical reaction dynamics simulation of hydrogen on a diamond-like carbon surface based on tight-binding quantum chemical molecular dynamics," *Journal of Physical Chemistry C*, vol. 115, no. 46, pp. 22981–22986, 2011.

[16] O. L. Eryilmaz and A. Erdemir, "On the hydrogen lubrication mechanism(s) of DLC films: an imaging TOF-SIMS study," *Surface and Coatings Technology*, vol. 203, no. 5–7, pp. 750–755, 2008.

[17] F. G. Sen, Y. Qi, and A. T. Alpas, "Surface stability and electronic structure of hydrogen-and fluorine-terminated diamond surfaces: a first principles investigation," *Journal of Materials Research*, vol. 24, no. 8, pp. 2461–2470, 2009.

[18] J. A. Johnson, J. B. Woodford, X. Chen, J. Andersson, A. Erdemir, and G. R. Fenske, "Insights into near-frictionless carbon films," *Journal of Applied Physics*, vol. 95, no. 12, pp. 7765–7771, 2004.

[19] A. Erdemir, "Developing a near-frictionless carbon coating," *Tribology and Lubrication Technology*, vol. 61, no. 10, pp. 12–14, 2005.

[20] J. A. Harrison, C. T. White, R. J. Colton, and D. W. Brenner, "Molecular-dynamics simulations of atomic-scale friction of diamond surfaces," *Physical Review B*, vol. 46, no. 15, pp. 9700–9708, 1992.

[21] M. Garvey, M. Weinert, and W. T. Tysoe, "On the pressure dependence of shear strengths in sliding, boundary-layer friction," *Tribology Letters*, vol. 44, no. 1, pp. 67–73, 2011.

[22] G. Zilibotti and M. C. Righi, "Ab initio calculation of the adhesion and ideal shear strength of planar diamond interfaces with different atomic structure and hydrogen coverage," *Langmuir*, vol. 27, no. 11, pp. 6862–6867, 2011.

[23] G. Gao, R. J. Cannara, R. W. Carpick, and J. A. Harrison, "Atomic-scale friction on diamond: a comparison of different

sliding directions on (001) and (111) surfaces using MD and AFM," *Langmuir*, vol. 23, no. 10, pp. 5394–5405, 2007.

[24] G. T. Wang, S. F. Bent, J. N. Russell Jr., J. E. Butler, and M. P. D'Evelyn, "Functionalization of diamon (100) by diels-alder chemistry," *Journal of the American Chemical Society*, vol. 122, no. 4, pp. 744–745, 2000.

[25] T. Halicioglu, "Calculation of surface energies for low index planes of diamond," *Surface Science*, vol. 259, no. 1-2, pp. L714–L718, 1991.

[26] R. H. Telling, C. J. Pickard, M. C. Payne, and J. E. Field, "Theoretical strength and cleavage of diamond," *Physical Review Letters*, vol. 84, no. 22, pp. 5160–5163, 2000.

[27] B. Delley, "An all-electron numerical method for solving the local density functional for polyatomic molecules," *The Journal of Chemical Physics*, vol. 92, no. 1, pp. 508–517, 1990.

[28] B. Delley, "A standard tool for density functional calculations: review and advances," in *Modern Density Functional Theory: A Tool for Chemistry*, J. M. Seminario and P. Politzer, Eds., vol. 2 of *Theoretical and Computational Chemistry*, Elsevier Science B, Amsterdam, The Netherlands, 1995.

[29] J. P. Perdew and Y. Wang, "Accurate and simple analytic representation of the electron-gas correlation energy," *Physical Review B*, vol. 45, no. 23, pp. 13244–13249, 1992.

[30] D. Henwood and J. D. Carey, "Ab initio investigation of molecular hydrogen physisorption on graphene and carbon nanotubes," *Physical Review B*, vol. 75, no. 24, Article ID 245413, 10 pages, 2007.

[31] S. K. Nayak, B. K. Rao, and P. Jena, "Equilibrium geometries, electronic structure and magnetic properties of small manganese clusters," *Journal of Physics Condensed Matter*, vol. 10, no. 48, pp. 10863–10877, 1998.

[32] T. Bučko, J. Hafner, S. Lebègue, and J. G. Ángyán, "Improved description of the structure of molecular and layered crystals: Ab initio DFT calculations with van der Waals corrections," *Journal of Physical Chemistry A*, vol. 114, no. 43, pp. 11814–11824, 2010.

[33] Y. Liu and W. A. Goddard, "First-principles-based dispersion augmented density functional theory: from molecules to crystals," *Journal of Physical Chemistry Letters*, vol. 1, no. 17, pp. 2550–2555, 2010.

[34] I. Mayer, "Bond orders and valences from ab initio wave functions," *International Journal of Quantum Chemistry*, vol. 29, no. 3, pp. 477–483, 1986.

[35] R. S. Mulliken, "Electronic population analysis on LCAO-MO molecular wave functions. II. Overlap populations, bond orders, and covalent bond energies," *The Journal of Chemical Physics*, vol. 23, no. 10, pp. 1841–1846, 1955.

[36] L. Ostrovskaya, V. Perevertailo, V. Ralchenko, A. Dementjev, and O. Loginova, "Wettability and surface energy of oxidized and hydrogen plasma-treated diamond films," *Diamond and Related Materials*, vol. 11, no. 3-6, pp. 845–850, 2002.

[37] G. Tanasa, *Atomic scale friction: a scanning probe study on crystalline surfaces [Ph.D. thesis]*, Eindhoven University of Technology, 2005.

[38] P. L. Piotrowski, R. J. Cannara, G. Gao, J. J. Urban, R. W. Carpick, and J. A. Harrison, "Atomistic factors governing adhesion between diamond, amorphous carbon and model diamond nanocomposite surfaces," *Journal of Adhesion Science and Technology*, vol. 24, no. 15-16, pp. 2471–2498, 2010.

[39] R. Neitola and T. A. Pakkanen, "Ab initio studies on the atomic-scale origin of friction between diamond (111) surfaces," *Journal of Physical Chemistry B*, vol. 105, no. 7, pp. 1338–1343, 2001.

[40] M. D. Perry and J. A. Harrison, "Universal aspects of the atomic-scale friction of diamond surfaces," *Journal of Physical Chemistry*, vol. 99, no. 24, pp. 9960–9965, 1995.

[41] W. Zhong and D. Tomãnek, "First-principles theory of atomic-scale friction," *Physical Review Letters*, vol. 64, no. 25, pp. 3054–3057, 1990.

[42] T. A. Albright, J. K. Burdett, and M. H. Whangbo, *Orbital Interactions in Chemistry*, John Wiley & Sons, New York, 1985.

[43] T. Çağin, J. Che, M. N. Gardos, A. Fijany, and W. A. Goddard, "Simulation and experiments on friction and wear of diamond: a material for MEMS and NEMS application," *Nanotechnology*, vol. 10, no. 3, pp. 278–284, 1999.

[44] Y. Mo, K. T. Turner, and I. Szlufarska, "Friction laws at the nanoscale," *Nature*, vol. 457, no. 7233, pp. 1116–1119, 2009.

[45] D. S. Grierson, E. E. Flater, and R. W. Carpick, "Accounting for the JKR-DMT transition in adhesion and friction measurements with atomic force microscopy," *Journal of Adhesion Science and Technology*, vol. 19, no. 3–5, pp. 291–311, 2005.

[46] E. C. Gage, T. W. Mcdaniel, W. A. Challener et al., "Heat assisted magnetic recording," *Proceedings of the IEEE*, vol. 96, no. 11, pp. 1810–1835, 2008.

[47] R. Z. Lei, A. J. Gellman, and P. Jones, "Thermal stability of Fomblin Z and Fomblin Zdol thin films on amorphous hydrogenated carbon," *Tribology Letters*, vol. 11, no. 1, pp. 1–5, 2001.